TRANSIENT GROWTH: EXPERIMENTS, DNS AND THEORY

F. Gökhan Ergin
Mechanical and Aerospace Engineering Department,
Case Western Reserve University
Cleveland, Ohio 44106, USA
gokhan@case.edu

Meelan Choudhari
Computational Modelling and Simulation Branch,
NASA Langley Research Center
Hampton, Virginia 23681, USA
m.m.choudhari@larc.nasa.gov

Paul Fischer
Mathematics and Computer Science Division,
Argonne National Laboratory
Argonne, Illinois 60439, USA
fischer@mcs.anl.gov

Anatoli Tumin
Department of Aerospace and Mechanical Engineering,
The University of Arizona
Tucson, Arizona 85721, USA
tumin@engr.arizona.edu

ABSTRACT

Transient growth of linearly stable disturbances is believed to play an important role in the subcritical transition of laminar boundary layers and the self-sustained nature of boundary layer fluctuations in a fully turbulent flow. Prior work on transient growth has focused on identifying the optimum initial disturbances that result in maximum transient growth. This paper addresses the companion issue of receptivity of those disturbances, the mechanism that determines the actual magnitudes of transient growth that are realized in a given physical situation. A synergistic combination of experimental, computational, and theoretical approaches is used to quantify the flow receptivity to surface roughness in a Blasius boundary layer. Results reveal the non-optimality of the transient growth factors involved as well as the sensitive dependence of flow perturbations to the geometric characteristics of the roughness distribution. Direct numerical simulations (DNS) are compared in detail with experimental results, results obtained from linear receptivity theory and optimal disturbance calculations. DNS shows good agreement with the experimental results. Differences between the linear theory and DNS are attributed to nonlinear receptivity mechanisms. Results also support the proposal by Fransson et al. (2004) that disagreement between optimal disturbances and experiments/DNS may be attributed to differences involving the wall normal location of the streamwise vortex initiating the transient growth.

INTRODUCTION

The transient growth phenomenon refers to an algebraic amplification of small-amplitude disturbances prior to an exponential decay farther downstream. Transient growth has been proposed as a likely mechanism behind laminar-turbulent transition scenarios that cannot be explained by the classical paradigm of hydrodynamic instabilities. Transient growth is also believed to play an important role in the self-generation of turbulence in fully turbulent wall shear flows (Butler and Farrell 1993; Chernyshenko and Baig 2005). Physically, the occurrence of transient growth can be explained by Landahl's (1980) "lift-up" mechanism, where a pair of stable, counter-rotating, streamwise-oriented vortices transfers momentum across the boundary layer, creating a significantly stronger streamwise velocity perturbation.

The mathematical foundation of transient growth has been described by Schmid and Henningson (2001) and Reshotko (2001). Transient growth arises because the linearized disturbance equations are not self-adjoint and, therefore, have nonorthogonal eigenmodes. In boundary layers, the correct representation of disturbances is the superposition of the discrete and continuous eigenmodes of the Orr–Sommerfeld (OS) equation. In classical linear stability analysis, the most amplified discrete eigenmode represents the dominant disturbance observed in an experiment. However, even in the subcritical region where the TS waves are damped, a suitable mixture of continuous spectrum modes (each of which has a different

decay rate) can exhibit temporary algebraic growth before the exponential decay manifests itself.

A particular combination of the modes will form an initial disturbance that experiences the maximum amount of growth. Such a disturbance is called the optimal disturbance (Farrell 1988) and many investigators have contributed to the modelling of spatially growing optimal disturbances (Andersson et al. 1999; Luchini 2000; Tumin and Reshotko 2001). For a laminar Blasius boundary layer, the optimal initial disturbance has been shown to consist of an array of stationary streamwise vortices with a dimensionless spanwise wavenumber of 0.45. Andersson et al. (1999) also found that the measured evolution of low-frequency boundary-layer disturbances excited via freestream turbulence is in agreement with the optimal growth theory. On the other hand, there is a significant mismatch between the optimal growth theory and measured (i.e. realizable) disturbances due to controlled surface roughness. White (2002) finds that roughness-induced disturbances show suboptimal behavior. Fransson et al. (2004) confirm this observation and attribute the mismatch to differences between the initial disturbance profiles used in optimal disturbance studies and those induced by surface roughness. The former corresponds to a streamwise vortex that is not confined to the boundary layer. Unlike the case of freestream turbulence, however, disturbances generated by low amplitude surface roughness are mostly confined to the boundary layer region.

Transient disturbances are extremely sensitive to initial disturbance conditions as these determine the spectrum of modes that make up the disturbance and, hence, its algebraic growth rate. Since the maximum disturbance energy attained downstream of the source is mostly specified by the algebraic growth rate, understanding the receptivity mechanism that determines the initial disturbance condition is crucial. The objective of this work is to summarize the recent progress in experimental, computational and theoretical investigations of roughness-induced transient growth, with an emphasis on detailed comparisons between the respective findings for specific roughness configurations. Remaining challenges to assessing the relevance of the optimal growth theory to roughness effects on boundary-layer transition are also outlined.

EXPERIMENTS

White and coworkers (White and Ergin 2003; White et al. 2005; Ergin and White 2005) at Case Western Reserve University (Case) have conducted a number of experiments on the behavior of roughness-induced transient disturbances. Present efforts are focused on generating disturbance data that is suitable for comparison with DNS and theoretical models. A brief description of the experimental setup and data analysis procedure is given below.

Measurements are obtained in the boundary layer of a flat plate with an elliptical leading edge and disturbances are generated by a spanwise array of cylindrical roughness elements. Roughness arrays provide considerable flexibility in varying the controlled disturbance inputs, via variations in the height, spacing and diameter of the roughness elements. Various averaging techniques, such as spatial phase-locked averaging, can be utilized to improve the signal-to-noise characteristics during data analysis. Throughout this paper, k denotes the roughness height, λ_k is the spanwise roughness spacing (19 mm), x_k is the array's streamwise location relative to the physical leading edge (300 mm), and Re_k is the roughness Reynolds number, $U(k)k/\nu$. Hotwire velocity measurements are performed in planes perpendicular to the streamwise flow. An illustration of the experimental setup is given in Figure 1.

The main data analysis technique is to decompose the kinetic energy associated with the steady disturbance into spanwise wavelength components by performing a spanwise Fourier transform, computing the energy of each and examining the downstream evolution of these energies. The energy is defined by

$$E_\lambda(x) = \int_0^\infty \mathrm{PSD}(x, \eta, \lambda) d\eta \qquad (1)$$

where PSD is the one-sided power spectral density.

For $Re_k = 202$, the phase-lock averaged steady streamwise velocity contours obtained 30 mm downstream of the roughness array are shown in Figure 2. In this figure, the flow is into the page; the abscissa is the spanwise coordinate normalized by λ_k, and the ordinate is the dimensionless wall-normal coordinate, η. The contour lines indicate 10% increments of the freestream velocity and the box in the middle approximates the planform shape of the cylindrical roughness element that generated this disturbance. The decelerated regions along the roughness centerline and accelerated regions along the edges agree well with previous experimental results. The measured streamwise velocity contours can be compared to DNS results which are shown in Fig. 3.

White and Ergin (2003) investigated how the steady disturbance energy in spatial wavelengths scales with roughness amplitude. For $Re_k = 119$ and a diameter of 6.35 mm (which corresponds to $\lambda_k/3$), Fig. 4 shows the downstream evolution of the steady disturbance energy contained in λ_k, $\lambda_k/2$, $\lambda_k/3$, and $\lambda_k/4$ components. It was found that the disturbance energy approximately scales with Re_k^2 (i.e., k^4), and this scaling is further verified by White et al. (2005) for Re_k ranging from 16 to 195. Rice (2004) extends the range to 254. Fig. 5 shows the transient growth of $E_{\lambda_k/3}$ for selected values of Re_k. In this figure, the solid lines denote the least squares fits to the data using the model function $a(x - x_k)\exp[-(x - x_k)/b]$.

White et al. (2005) also considered the effect of roughness diameter on disturbance energy and found that even a small change in roughness diameter had a dramatic effect on the disturbance spectrum, both quantitatively and qualitatively. The effect of roughness diameter on the downstream evolution of $E_{\lambda_k/3}$ is shown in Fig. 6, where the solid line is an interpolation of 6.35-mm diameter for $Re_k = 177$. In this figure, the 6.35- and 7.62-mm-diameter roughness produce transient growth, 4.76- and 5.08-mm-diameter roughness produce an initial decay followed by transient growth, and 3.81-mm-diameter roughness produce pure decay. These findings indicate that both height and shape are equally important in the receptivity of roughness-induced transient disturbances.

Tumin (2003) proposed a multimode decomposition method that addresses the receptivity problem for spatially growing realistic perturbations. Quantification of the initial disturbance profile for comparison with this theory requires the measurement of all three disturbance velocity components. Ergin and White (2005) took the first step in obtaining the complete velocity field by measuring the spanwise and streamwise velocity components. At present, spanwise velocity measurements are too limited for comparison with numerical works. Continuing efforts are focused on obtaining extensive streamwise and spanwise velocity measurements so

that a definitive comparison can be made. Multicomponent velocity measurements are crucial to an improved understanding of transient disturbances, because of their relevance to the streamwise oriented steady vortical structures that initiate transient growth.

DIRECT NUMERICAL SIMULATIONS

Fischer and Choudhari (2004) have carried out numerical simulations for various roughness configurations that enable detailed comparisons with the measurements of White and Ergin (2003). The unsteady incompressible Navier–Stokes equations were integrated in time by using the spectral element discretization in space and a third-order, operator-splitting formulation in time. After initial simulations with a full wavelength domain to confirm the spanwise symmetry of the flow field, the remaining simulations were performed using half the wavelength along the spanwise direction. Grid convergence of the computational results was confirmed by varying the order of the discretization polynomial within each element.

For $Re_k = 119$, Fischer and Choudhari (2004) examined the downstream evolution of the relevant spanwise harmonics of the disturbance field. The agreement between the experimentally measured and numerically computed modal energies can be observed by comparing Fig. 7 with Fig. 4. The initial rapid decay of the λ_k; the transient growth of λ_k, $\lambda_k/3$, and $\lambda_k/4$; and the monotonic decay of $\lambda_k/2$ are all captured in the simulations. In Fig. 7, the numerically determined streamwise locations where the fundamental mode, λ_k reaches a minimum, where $\lambda_k/3$, and $\lambda_k/4$ modes reach their respective peak amplitudes, and where the downstream decay rate of the $\lambda_k/2$ mode changes are almost exactly equal to their experimentally measured counterparts. Minor differences are observed in the far wake region of the fundamental mode. The modal energy computed using DNS overestimates the corresponding modal energy measured in the experiments (modal energies can be obtained from the experimental data by integrating E_λ over one unit of inverse wavelength). Numerical results for other roughness heights are consistent, in general, with the observed nonlinear scaling of disturbance amplitudes and the approximate range of Re_k over which this scaling has been observed.

Figure 8 compares the downstream evolution of steady disturbance energy obtained by experiments and DNS for $Re_k = 119$. The disturbance energy at each x location is computed by integrating the spanwise variance of the steady velocity disturbance from the wall to the freestream. This figure shows good agreement between the approaches with both indicating an initial rapid decay region, a slow but clear growth region and finally a weak decay region in the x direction.

One of the advantages of DNS is the readily available pressure field, which cannot be easily measured in the experiments. Figure 9 shows the salient features of the near-wall flow field in the near vicinity of roughness element for $Re_k = 119$. The bottom half of the figure displays the surface pressure contours. One observes peak pressures along the centerline just ahead of the roughness element, lowest pressure above the roughness (not shown in the figure), and a monotonic pressure recovery in the wake region, all in agreement with the previous works. The upper half depicts the distribution of streamwise velocity and the streamlines at a small fixed height just above the surface. The top half of the figure clearly highlights the two separate regions of flow reversal - a primary region behind the roughness element and a smaller region near the centerline just in front of the element.

THEORETICAL ANALYSIS

A theoretical analysis of perturbations generated by a roughness element was presented in Tumin and Reshotko (2004) who considered the linearized Navier–Stokes equations and linearized boundary conditions. The method was based on an expansion of the solution into the normal modes of the continuous spectrum and amplitudes were calculated using the biorthogonal eigenfunction system (Tumin 2003). The linear approach is limited to small roughness elements with heights less than the viscous sublayer thickness. In the present experiments and computations, the roughness height exceeds this by a significant margin. As follows from the high Reynolds number asymptotic theory (Smith et al. 1977), the governing equations are linear in the boundary layer's main deck, but nonlinear in the vicinity of the wall. The experimental and computational data demonstrate that the velocity perturbation amplitudes scale with Re_k (i.e., k^2), illustrating the nonlinear character of the receptivity problem.

In order to assess the difference between the linear and nonlinear receptivity mechanisms, we compare the numerical results for $Re_k = 119$ based on the linear theory (Tumin and Reshotko 2004) with DNS results and optimal perturbations. Figures 10 and 11 show a comparison of the wall-normal and the spanwise velocity components of the fundamental mode at $x = 335$ mm. In both figures, the v and w profiles computed using each approach are normalized by the same factor such that the near-wall maximum w velocity computed using each method is unity. One can see that the velocity perturbations computed using linear receptivity theory are localized closer to the wall than the DNS perturbations, and the DNS perturbations are closer to the wall in comparison with the conventional optimal perturbation.

In spite of the nonlinear character of the receptivity phenomenon, the downstream perturbations are small enough, such that their dynamics in the transient growth region can be described within the scope of the linearized Navier–Stokes equations. The observed transient growth effect differs from the theoretical prediction based on the optimal perturbation concept. To assess the difference between the optimal velocity perturbations and the perturbations generated by the roughness array, we have calculated the optimal profiles corresponding to the maximum energy growth for the λ_k component over the limited range of $x = 335$ mm to $x = 700$ mm. Figs. 10 and 11 confirm that the optimal perturbations are spread farther away from the wall than the DNS profiles for the particular roughness configuration examined herein.

CONCLUSIONS

The recent developments in transient growth research obtained using experimental, theoretical and computational approaches are presented. Experimental results show that disturbances generated by surface roughness are non-optimal and the DNS simulations are in satisfactory agreement with the measured data. Non-optimality is attributed to the fact that the disturbance generated by the roughness element involves a streamwise-oriented vortex that is closer to the surface than the streamwise vortex predicted by optimal disturbance calculations. The experiments and simulations also establish that

the disturbance velocity scales approximately with the square of the roughness height and that the roughness shape also has an important influence on the receptivity of roughness-induced disturbances. The dependence on roughness height shows that the receptivity mechanism is nonlinear, which implies that linear receptivity models are not appropriate for the roughness amplitudes considered here. Despite the fact that the receptivity is nonlinear, the downstream perturbations in the transient growth region are small and, hence, their evolution should be well approximated by the linearized Navier–Stokes equations. Consequently, the multimode decomposition technique (Tumin 2003) can be applied to analyze the DNS and the experimental data, providing a quantitative description of the perturbations as a sum of the continuous spectrum normal modes. This technique requires the measurement of the complete velocity field in the near wake. Current experimental efforts are focused on supplying this data by measuring the w and u velocities and estimating the v velocity using continuity. This data, in conjunction with the biorthogonal decomposition technique, will lead to receptivity models for non-optimal initial disturbances which will be useful for predicting transition in situations with significant roughness-induced transient growth.

ACKNOWLEDGMENTS

The authors wish to thank Prof. Edward White for many valuable comments and suggestions. FGE acknowledges the Air Force Office of Scientific Research for its support through grant number F49620-02-1-0058 and the Case School of Engineering for its support through a Case Prime Fellowship. Computational resources for the DNS were provided both by NASA and the Department of Energy. AT acknowledges the Air Force Office of Scientific Research for its support through grant number F33615-98-D-3601.

REFERENCES

Andersson, P., M. Berggren, and D. S. Henningson (1999). Optimal disturbances and bypass transition in boundary layers. *Phys. Fluids 11*(1), 134–150.

Butler, K. and B. Farrell (1993). Optimal perturbations and streak spacing in wall-bounded turbulent shear flow. *Phys. Fluids A 5*(3), 774–777.

Chernyshenko, S. I. and M. F. Baig (2005). Streaks and vortices in near-wall turbulence. *Phil. Trans. Royal Soc. A*. To appear.

Ergin, F. G. and E. B. White (2005). Multicomponent and unsteady measurements of transient disturbances. AIAA Paper 2005-0527.

Farrell, B. F. (1988). Optimal excitation of perturbations in viscous shear flow. *Phys. Fluids 31*, 2093.

Fischer, P. and M. Choudhari (2004). Numerical simulation of roughness-induced transient growth in a laminar boundary layer. AIAA Paper 2004-2539.

Fransson, J. H. M., L. Brandt, A. Talamelli, and C. Cossu (2004). Experimental and theoretical investigation of the non-modal growth of steady streaks in a flat plate boundary layer. *Phys. Fluids 16*(10), 3627–3638.

Landahl, M. T. (1980). A note on an algebraic instability of inviscid parallel shear flows. *J. Fluid Mech. 98*, 243–251.

Luchini, P. (2000). Reynolds-number-independent instability of the boundary layer over a flat surface: Optimal perturbations. *J. Fluid Mech. 404*, 289–309.

Reshotko, E. (2001). Transient growth—A factor in bypass transition. *Phys. Fluids 13*(5), 1067–1075.

Rice, J. M. (2004). Roughness receptivity and scaling of non-optimal transient disturbances. Master's thesis, Case Western Reserve University.

Schmid, P. J. and D. S. Henningson (2001). *Stability and transition in shear flows*. New York: Springer.

Smith, F. T., R. I. Sykes, and P. W. M. Brighton (1977). A two-dimensional boundary layer encountering a three-dimensional hump. *J. Fluid. Mech. 83*, 163–176.

Tumin, A. (2003). Multimode decomposition of spatially growing perturbations in a two-dimensional boundary layer. *Phys. Fluids 15*(9), 2525–2540.

Tumin, A. and E. Reshotko (2001). Spatial theory of optimal disturbances in boundary layers. *Phys. Fluids 13*(7), 2097–2104.

Tumin, A. and E. Reshotko (2004). The problem of boundary-layer flow encountering a three-dimensional hump revisited. AIAA Paper 2004-0101.

White, E. B. (2002). Transient growth of stationary disturbances in a flat plate boundary layer. *Phys. Fluids 14*(12), 4429–4439.

White, E. B. and F. G. Ergin (2003). Receptivity and transient growth of roughness-induced disturbances. AIAA Paper 2003-4243.

White, E. B., J. M. Rice, and F. G. Ergin (2005). Receptivity of stationary transient disturbances to surface roughness. *Phys. Fluids 17*(5). In press.

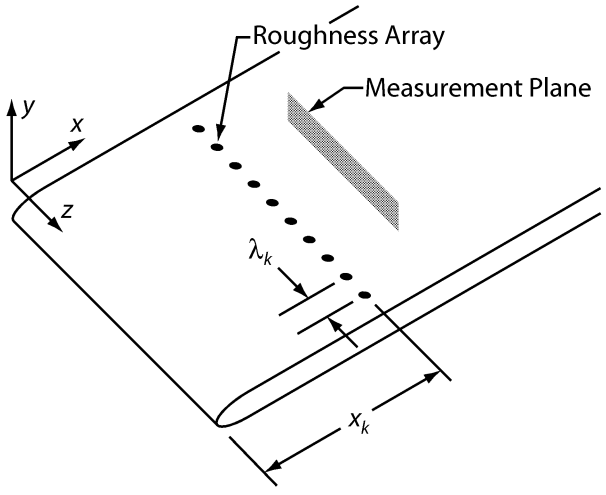

Figure 1: Schematic view of the flat plate model and roughness array.

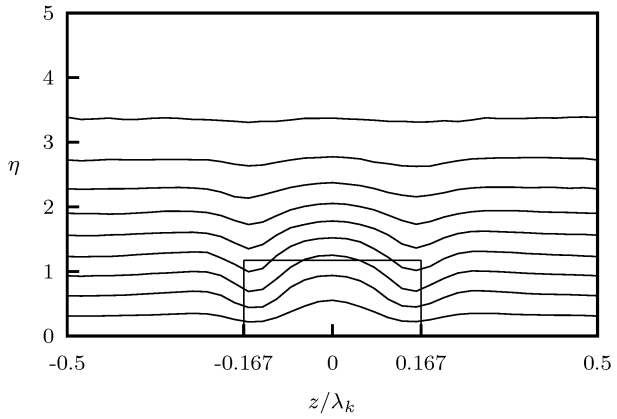

Figure 2: Experimentally measured streamwise velocity contours for $x = 330$ mm, $Re_k = 202$.

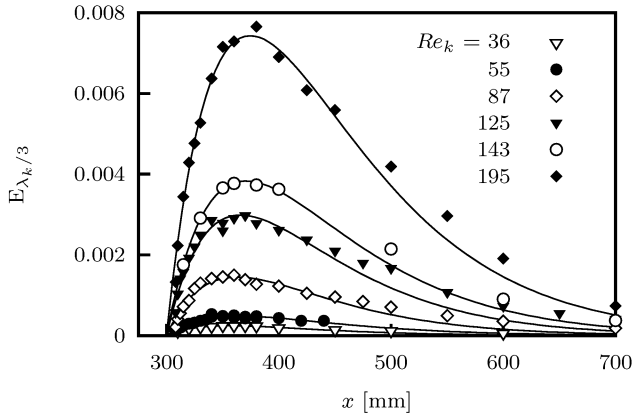

Figure 5: Transient growth of disturbance kinetic energy contained in $\lambda_k/3$ for various roughness heights. $d = 6.35$ mm.

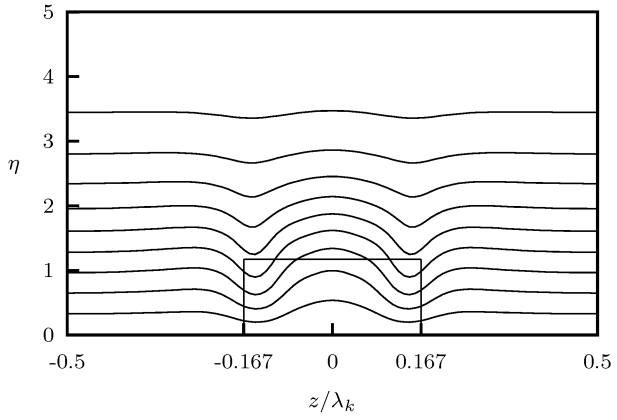

Figure 3: Numerically calculated streamwise velocity contours for $x = 330$ mm, $Re_k = 202$.

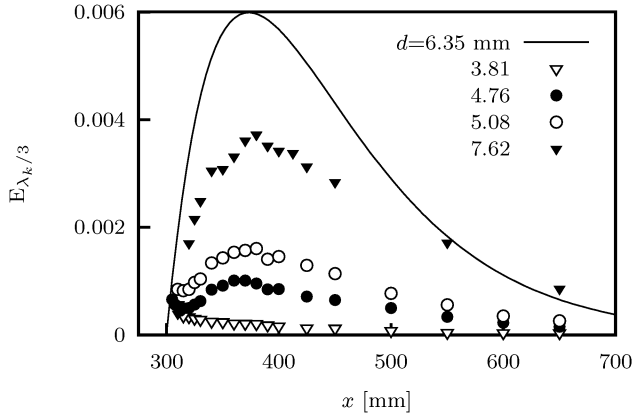

Figure 6: Evolution of disturbance kinetic energy contained in $\lambda_k/3$ for various roughness diameters. $Re_k = 177$.

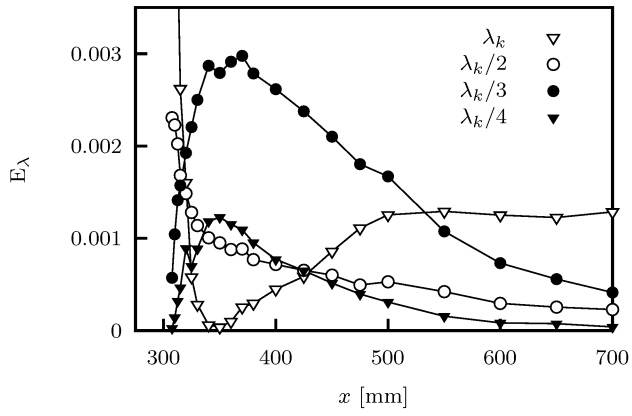

Figure 4: Streamwise evolution of E_λ measured by White and Ergin (2003) for $Re_k = 119$.

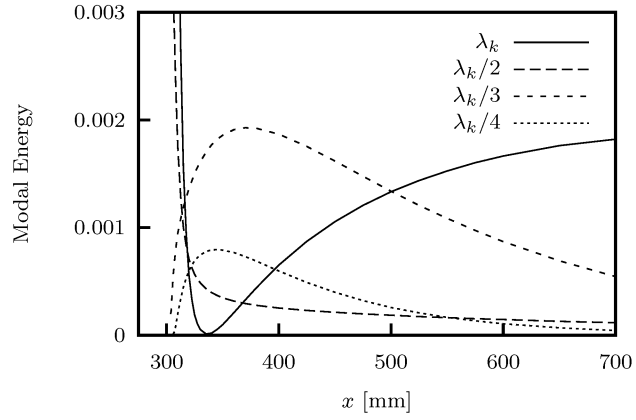

Figure 7: Streamwise evolution of modal energies computed by Fischer and Choudhari (2004) for $Re_k = 119$.

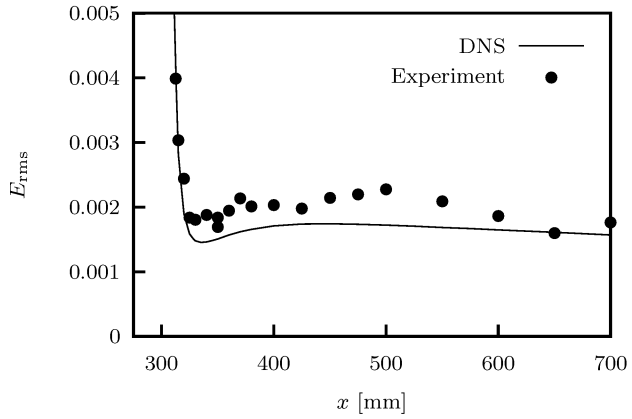

Figure 8: Downstream evolution of steady spanwise rms disturbance energy, $E_{\rm rms} = \int_0^\infty {U'_{\rm rms}}^2 d\eta$ for $Re_k = 119$.

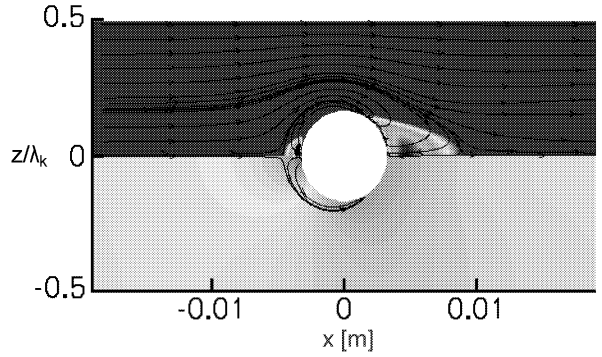

Figure 9: Flow features in the vicinity of a roughness element: surface pressure distribution (lower half); streamwise shear stress and streamlines (upper half).

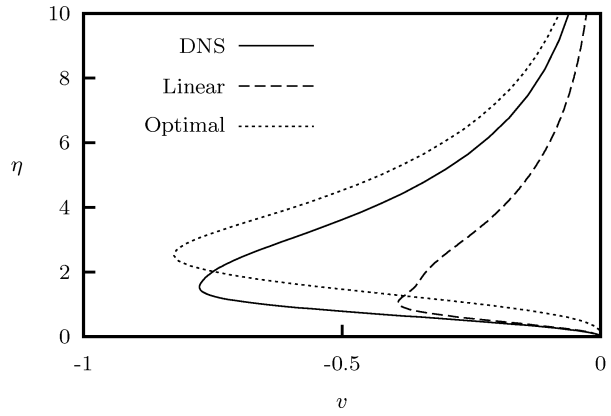

Figure 10: Comparison of wall-normal velocity profiles for $x = 335$ mm, $Re_k = 119$.

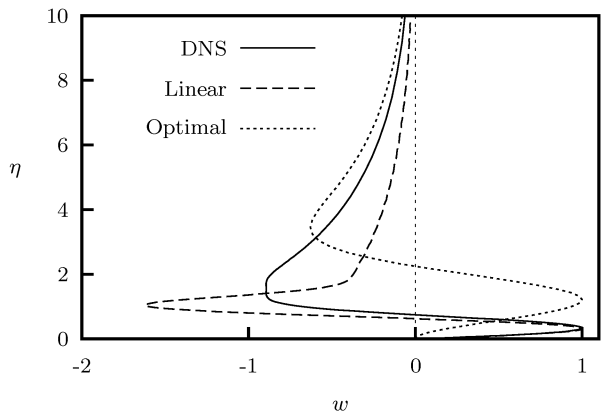

Figure 11: Comparison of spanwise velocity profiles for $x = 335$ mm, $Re_k = 119$.